Acoustic emission-based damage characterization of 70 MPa type IV hydrogen composite pressure vessels during hydraulic tests

Liao, B. B.; Wang, D. L.; Hamdi, M.; Zheng, J. Y.; Jiang, P.; Gu, C. H.; Hong, W. R.

DOI
10.1016/j.ijhydene.2019.02.217

Publication date
2019

Document Version
Accepted author manuscript

Published in
International Journal of Hydrogen Energy

Acoustic emission-based damage characterization of 70 MPa Type IV hydrogen composite pressure vessels during hydraulic tests

B.B. Liao [a], D.L. Wang [a], M. Hamdi [b], J.Y. Zheng [a,c *], P. Jiang [a,d *], C.H. Gu [a], W.R. Hong [a]

a. Institute of Process Equipment, Zhejiang University, Hangzhou 310027, China
b. Structural Integrity & Composites Group, Faculty of Aerospace Engineering, Delft University of Technology, Kluyverweg 1, 2629 HS Delft, The Netherlands

c. State Key Laboratory of Fluid Power and Mechatronic Systems, Zhejiang University, Hangzhou 310027, China
d. Northeast Petroleum University, Heilongjiang Daqing 163318, China

Abstract: This paper aims to apply an acoustic emission (AE) method to characterize the damage mechanisms of composite hydrogen pressure vessels (Type IV) with a service pressure of 70 MPa. First, AE signals were captured during the multi-step loading of two vessels. Second, AE feature parameters in time-domain and frequency-domain analyses such as amplitude, frequency, and energy were studied. A multi-parameter statistical analysis (MPSA) method based on empirical mode decomposition (EMD) and *K*-means algorithm was performed to cluster AE events. Intrinsic mode functions (IMFs) were decomposed by EMD and three IMFs with high frequency were chosen to reconstruct the feature parameters and provide signal pre-processing for *K*-means clustering analysis. Based on the relationship between AE features and the damage modes, three main clusters with distinguished amplitude, absolute energy, and energy were correlated to matrix cracking, fiber-matrix debonding, and fiber breakage. Besides, the effectiveness of MPSA method for signal classification is validated by principal component analysis (PCA) and fast Fourier transformation (FFT) methods. Finally, the AE parameters of the damages modes, such as amplitude and counts to peak, were studied for both the hydraulic proof test and the burst test. This allows the determination of the changes in the damage mechanisms with increasing pressure. Results show that AE method can be reliably used to characterize the mechanisms of burst damage in composite pressure vessels.

Keywords: composite hydrogen pressure vessel; hydraulic tests; acoustic emission; damage modes recognition;

*Corresponding author. E-mail: jyzh@zju.edu.cn (J.Y. Zheng); jpnepu@163.com (P. Jiang); Tel: 86-571-87952110

1. Introduction

Conventional energy sources like fossil fuel are increasingly replaced by alternative sources such as hydrogen. One of the main sectors benefiting from this new promising source is the automotive industry, where various hydrogen storage methods have been developed [1,2]. For instance, composite pressure vessels with metal (Type III) and non-metal (Type IV) liners are commonly employed in this sector for high-pressure hydrogen storage. This is due to their good strength, stiffness-to-weight ratio, fatigue performance, and corrosion resistance [3]. Furthermore, the design and manufacture of these vessels are enhanced by newly-advanced filament wound technologies [4].

During the past decades, a large number of experimental [5-7] and numerical [8-11] studies have explored the structural response of hydrogen composite pressure vessels. These studies showed that the failure mechanism of the vessels is not abrupt but rather progressive depending on the accumulated internal pressure. It consists of several modes such as matrix cracking, fiber-matrix interface debonding, and fiber. Therefore, monitoring and analyzing the damage evolution in composite pressure vessels is important to assess their structural integrity. Also, vessels employed for hydrogen storage are significantly susceptible to various damages such as abrasion, scratch, impact, and aging [12], which reduces their load capacity and fatigue performance [13]. This necessitates the regular inspection of composite pressure vessels to ensure their safety.

Recently, a periodic inspection of composite pressure vessels was conducted according to ISO 11623 standard using hydraulic proof test and internal and external visual inspections [14]. However, this manual method is costly and time-consuming because it includes multiple inspection steps. It also relies on subjective judgements, which may lead to high result variability. To overcome these limitations, several non-destructive methods including ultrasonic scan [12], X-ray tomography [12], and acoustic emission (AE) [15] were employed. Particularly, AE-based approach, conducted by implementing many sensors on the whole vessel, provided promising results..

Accurate assessment criteria should be followed while inspecting composite hydrogen pressure vessels using AE techniques. To fulfill this purpose, damage mechanisms should be

first identified and correlated to AE features. This was the objective of several AE studies previously performed on composite pressure vessels [12,16,17]. AE methods were used to detect the damage caused by constant and cyclic internal gas pressure loading [16], explore the thermo-mechanical properties under hydraulic and atmospheric fatigue cycling [17], and evaluate the damage status during hydrogen filling process [12]. However, these studies fell short in characterizing the damage modes and evolution mechanisms on the composite vessels.

Previous studies characterized the damage mechanisms on composite laminates using different analytical algorithms and AE parameters such as amplitude, absolute energy, and energy [18-24]. It is found that each damage mechanism is associated with a specific AE feature parameters [18,19]. For instance, critical AE signals were previously identified using Kohonen's self-organizing map which is based on neural network algorithm [20,21]. Despite its high accuracy, the neural network approach requires significant computational time and depends on the structure of the network and the number of the neurons. In another study, empirical mode decomposition (EMD) and Hilbert-Huang spectral analysis were used to obtain the frequencies associated with the composite damage mechanisms [22]. Similarly, Li et al. [23] identified the damage modes of composite laminates based on *K*-means algorithm. To improve the recognition process of the damage mechanisms, Marec et al. [24] used fuzzy *c*-means clustering method combined with principal component analysis (PCA). They showed that PCA method is a promising and consistent approach.

The main objective of the current study is to use AE methods to characterize the damage mechanisms of Type IV composite pressure vessels used for hydrogen storage under a service pressure of 70 MPa. Based on a multistep loading approach, AE signals were detected on two vessels with hydraulic pressure ranges of 0-105 MPa and 0-158 MPa, respectively. Then, AE parameters, namely amplitude, frequency, and energy, were studied. The change in damage mechanisms was obtained by increasing the pressure during the hydraulic proof test and burst test. The clustering of AE events was performed using a multi-parameter statistical analysis (MPSA) based on empirical mode decomposition (EMD) and *K*-means algorithm. The characteristic parameters of the resulting clusters (i.e. amplitude, absolute energy, and energy) were mainly correlated to the composite damage mechanisms (i.e. matrix cracking, fiber-matrix interface debonding, and fiber breakage). To validate the effectiveness of the MPSA method,

PCA analysis and fast Fourier transformation (FFT) were conducted.

2. Experimental procedures

2.1 Model systems

The model systems used in the experimental tests consist in two Type IV composite hydrogen pressure vessels. The vessels were manufactured using high strength carbon fiber-epoxy layers wrapped on a polyamide liner. They have a capacity, length, external diameter, and wall thickness of 42 L, 900 mm, 310 mm, and 26 mm, respectively. The service pressure is 70 MPa. Before conducting the experimental tests, the two vessels were both used for hydrogen storage onboard one fuel cell vehicle for 46500 kilometers, and then subjected to hydraulic fatigue tests of 5500 and 7500 cycles, respectively.

2.2 Test methods

Hydraulic proof test and burst test were conducted on the model systems with respect to GTR-13 standard [25]. They were performed using the multifunctional pressure test system with a pressure increase rate of approximately 0.1 MPa/s shown in Fig.1a, whose maximum pressure is 200 MPa. According to this standard, hydraulic proof pressure and minimum burst pressure should be 1.5 times and at least 2.25 times the service pressure, respectively. Thus, the pressure ranges of these two tests for each vessel are 0-105 MPa and 0-158 MPa respectively, as shown in Table 1.

A multi-step approach was followed to apply the pressure during the experimental tests. Each step consists of four phases, namely pressure increasing, pressure holding, pressure unloading, and pressure holding. The holding time of the constant pressure is 4 minutes. The pressure steps of the 0-105 MPa hydraulic proof test are shown in Fig.1b. Ten steps with a pressure increase of 10.5 MPa per step were considered in the hydraulic proof test. Similarly, multi-step loading method was also used in 0-158 MPa burst tests as shown in Fig.1c. The AE signals were detected at the pressure holding phase because the noise caused by the water-filling process is avoided during this phase. To avoid the destruction of the AE monitoring system during the burst test, AE signals were recorded to a minimum burst pressure of 158 MPa, then AE sensors and other devices were removed during the pressure unloading phase and the vessels were re-pressurized to burst.

2.3 AE monitoring

The AE monitoring system used in this study was supplied by Physical Acoustic Corporation (PAC). It includes an AE software, namely AEWin, and eight-channel data acquisition module to record the AE signals. Eight wide band piezoelectric transducers with a frequency range of 100-900 kHz were used as AE sensors. Their surfaces were covered by high-vacuum silicone grease for good acoustic coupling with the vessels. To filter the background noise, a threshold value of 40 dB was considered. For each sensor, the AE signals were calibrated using standardized pencil-lead breakage test commonly known as Hsu-Nielsen test. Then, AE signals were detected and amplified by preamplifiers with a fixed gain of 40 dB. Also, the AE monitoring system was connected to the multifunctional pressure system through pressure transducers to obtain pressure values and AE signals simultaneously. A tested vessel with the mounted sensors and preamplifiers is highlighted in Fig.2a. The layout of the sensors on the composite pressure vessels is shown in Fig.2b: six sensors were placed on the cylindrical part of the vessels and two on the upper and bottom heads. Each three of the eight sensors formed a triangular array according to stagger arrangement.

3. Clustering analysis method

3.1 MPSA method

3.1.1 EMD process

EMD process was used to (1) decompose complicated AE signals into finite IMFs, (2) remove the noise disturbance, and (3) extract AE features [26,27]. Based on these features, a reconstructed signal will be used for *K*-means clustering analysis. Also, the IMF functions were used to identify instantaneous frequencies. Each function is noted as $c_k(t)$ where $k \in [1, n]$ and corresponds to a specific component of the original signal [27,28]. According to previous studies, IMF functions should satisfy two main conditions [27,28]: first, the number of extrema and that of zero-crossings must be either equal or different in only one value. Second, the mean envelope value defined by local extrema should vanish at any point. Following EMD analysis, IMF extraction process from a signal $X(t)$ is described as follows [27,28]:

- Local extrema are connected through splines to form the upper and lower envelopes,

whose mean is noted as $m_1(t)$.

- The parameter $h_1(t)$ is defined as follows:

$$h_1(t) = X(t) - m_1(t) \quad (1)$$

If $h_1(t)$ satisfies the two IMF criteria above, then the first IMF component $c_1(t)$ is obtained and given by $c_1(t) = h_1(t)$. Otherwise, $h_1(t)$ is treated as a new data in the subsequent sifting process.

- The sifting process is repeated for p iterations. considering $h_{1p}(t)$ as:

$$h_{1p}(t) = h_{1(p-1)}(t) - m_{1p}(t) \quad (2)$$

If $h_{1p}(t)$ satisfies the two IMF criteria above, then the first IMF component $c_1(t)$ is $c_1(t) = h_{1p}(t)$.

- The residue $r_1(t)$ is defined as:

$$r_1(t) = X(t) - c_1(t) \quad (3)$$

This parameter is treated as the new data to be subjected to the same sifting process described above and will be used to get the second IMF component $c_2(t)$.

- The sifting process is finished when one of these conditions is met: (1) the residue $r_n(t)$ becomes a monotonic function (2) $c_n(t)$ or $r_n(t)$ is less than a predetermined value.

Thus, the original signal $X(t)$ can be expressed in terms of IMF components $c_k(t)$ $(i = 1,2,...,n)$ and final residue $r_n(t)$ as follows [27-29]:

$$X(t) = \sum_{k=1}^{n} c_k(t) + r_n(t) \quad (4)$$

3.1.2 K-means algorithm

K-means algorithm is a clustering method that assigns *m* input vectors $(y_1, y_2, ..., y_m)$ to *k* clusters $(B_1, B_2, ..., B_k)$, where each vector is allocated to the nearest cluster center [20,30]. The clustering process implemented by this algorithm is described as follows: First, the cluster center B_i is randomly initialized. Then, the distance between B_i and each input vector is computed and the input vectors are assigned to the nearest cluster center. Afterwards, new B_i locations are recalculated for the new clusters. Finally, the second and third steps are repeated until B_i locations do not change anymore.

This algorithm should be performed for different *k* values because the cluster number is

unknown. Also, a previous study showed that good partitioning is defined by Davis-Bouldin (DB) criterion expressed as follows [20]:

$$DB = \frac{1}{k}\sum_{i=1}^{k}\max_{i\neq j}\left\{\frac{s_i + s_j}{d_{ij}}\right\} \tag{5}$$

where d_{ij} corresponds to the distance between the centers of clusters i and j, and s_i and s_j are the distances of each input vector to cluster centers i and j, respectively. Low DB index values indicate good clustering.

3.2 Validation of the clustering analysis

To verify the validity of the clustering algorithm, signals separated by MPSA clustering process were visualized using principal component analysis [30,31]. PCA is a multivariate method that significantly reduces the dataset dimensions to improve data visualization. The dataset is transformed to new uncorrelated variables known as principal components. The principal components are determined through the eigenvectors in the covariance matrix with the highest eigenvalues.

Let X denotes the $n\times m$ input dataset where n and m are the number of AE signals and related AE features, respectively. First, the dataset should be standardized so all the variables have the same weight [30,31]. This is achieved by converting all data to have a zero mean and a unit standard deviation. Then, the covariance matrix C and the correlative eigenvalues $\lambda_i \ \left(i = 1,2,\cdots,m\right)$ are determined [30,31]. The resultant eigenvectors correspond to the columns of the matrix A given by $C = ADA^T$, where

$$D = \begin{bmatrix} \lambda_1 & 0 & \cdots & 0 \\ 0 & \lambda_2 & \cdots & 0 \\ \cdots & \cdots & \cdots & \cdots \\ 0 & 0 & 0 & \lambda_m \end{bmatrix} \quad \text{with} \quad \lambda_1 \geq \lambda_2 \geq \ldots \geq \lambda_m \tag{6}$$

The principal components are transformed by the first l eigenvectors, which are expressed as Eq. (7).

$$y = XA_l \tag{7}$$

The fast Fourier transformation can transform time-domain information to frequency-domain information. This method will be used to validate the frequency range associated with specific damage mechanism for the MPSA clustering results. More details about FFT method can be found in the literature [32].

3.3 Analysis procedure for AE signals

To characterize the damage modes induced by the hydraulic tests, an AE technique was employed and ten AE parameters were selected. They consist in seven time-domain parameters (amplitude, rise time, counts, duration, counts to peak, energy, and absolute energy) and three frequency-domain parameters (initiation frequency, average frequency, and peak frequency).

Initially, AE signals cannot be classified and analyzed because they are highly discrete and randomly distributed. To extract meaningful results, they should be treated using efficient analytical tools. In our study, MPSA method was adopted for damage mode recognition following the steps highlighted in Fig.3. First, the original signals are decomposed from high frequency to low frequency using EMD algorithm. The three IMFs with the highest frequencies are chosen to reconstruct the waveform information. Then, *K*-means algorithm was employed to conduct the clustering analysis and recognize the damage mode for the regenerated feature parameters after the correlation analysis. Finally, PCA and FFT methods were used to validate the results.

4. Results and discussion

4.1 Recognition of the damage modes

4.1.1 EMD decomposition of the AE signals

The AE signals obtained during the hydraulic tests were decomposed using EMD method. The resultant IMF functions are shown in Fig.4. The low, middle, and high amplitude signals of 45 dB, 70 dB, and 89 dB are selected for these examples. Given that EMD process follows an adaptive decomposition with intrinsic timescales, each IMF function exhibits a particular timescale modal and no inter-modal aliasing was obtained. Therefore, different IMF scales range from high frequency to low frequency as shown in Fig.4. In this figure, the most important functions are IMF-1, IMF-2, and IMF-3 because they consider high-frequency components and significant proportion of all the frequencies in the original signal. Therefore, these functions were selected to accurately determine AE feature parameters and effectively eliminate modal interference with low-frequency components. Then, their components were chosen to reconstruct the feature parameters and provide signal pre-processing for subsequent *K*-means clustering analysis. Each feature parameter in the time and frequency domains has some

information about the AE signals. If these parameters are not selected properly, the damage recognition process will be affected by redundant information. Thus, amongst the ten parameters obtained using the EMD reconstruction process, appropriate features were selected and redundant features were eliminated by commonly-used linear correlation analysis. Absolute energy-amplitude and counts to peak-energy were selected for the clustering analysis due to their low correlation coefficient.

4.1.2 K-means clustering analysis

To choose the appropriate number of clusters, DB index values of *K*-means clustering analysis were computed. DB index values of V1-H, V1-B, V2-H and V2-B tests on the two vessels are shown in Fig.5. The lowest DB index is obtained for three clusters for both hydraulic proof test and burst test. Thus, this number of clusters was selected for the *K*-means clustering analysis conducted in this paper.

As shown in Fig.6, the correlated distribution of the amplitude and absolute energy are studied for the vessels. In this figure, CL-1, CL-2 and CL-3 designate the clustering results of AE signals during all the constant pressure phases of the multistep pressure tests. For instance, for CL-1 cluster of the vessel V1-H, the ranges of the amplitude and absolute energy are 40-55 dB and 0-2×10^3 aJ, respectively. Similarly, those of CL-2 cluster are 50-72 dB and 2×10^3-4×10^4 aJ, consecutively. For CL-3 class, the amplitude is within 70-90 dB and the absolute energy is higher than that of CL-1 and CL-2 classes.

Similarly, Fig.7 shows the correlated distributions between the counts to peak feature and the energy feature. For example, for V1-H test, the energy range for CL-1 and CL-2 are 0-10 and 10-100, consecutively. For CL-3, the energy is greater than 100 (the energy in AE technique has no unit). This figure shows that the distribution ranges of counts to peak for CL-1, CL-2, and CL-3 clusters are not significantly different. Based on the results of *K*-means clustering analysis, the number of clusters is in good agreement for both the hydraulic proof test and burst test.

Tables 2 and 3 summarize the ranges of the amplitude, absolute energy, and energy values for the three clusters observed in hydraulic proof test and burst test for the two vessels. These are the time-domain results of the correlated distributions of amplitude-absolute energy and counts to peak-energy presented above. It is observed that CL-1 and CL-3 have the lowest and

highest amplitude, absolute energy, and energy, respectively. The tables also show that the amplitude, absolute energy, and energy cluster boundaries are about 65 dB, 2×10^3 aJ, and 20 between CL-1 and CL-2, and about 75 dB, 5×10^4 aJ, and 100 between CL-2 and CL-3. There are only a few changes in the distributions of the three clusters for the two vessels due to differences in pressure and fatigue cycles.

According to previous studies, three predominant damage mechanisms were observed in fiber-reinforced composites: matrix cracking, fiber-matrix debonding, and fiber breakage [22,24]. It is also found that the AE signals associated with matrix damage generally correspond to low amplitude and energy values in the ranges of 40-60 dB and 0-2×10^3 aJ, consecutively [33,34]. Similarly, those associated with fiber breakage correspond to high amplitude and energy values in the range of 80-100 dB and above 2.5×10^4 aJ, respectively. And the signal strength and distribution range of the fiber/matrix debonding signals are between the matrix cracking and fiber breakage signals [33-35]. Considering the energy and amplitude values of three different clusters presented in Tables 2 and 3, it is concluded that CL-1, CL-2, and CL-3 clusters mainly correspond to matrix cracking, fiber-matrix debonding, and fiber breakage damages, respectively.

4.1.3 Validation of the clustering results

In order to validate the effectiveness of the clustering algorithm, PCA analysis was used to obtain two-dimensional visualizations of *K*-means clustering results. AE signals are separated by three principal components PCA 0, PCA 1 and PCA 2. The scatter plot is mapped onto the PCA 0 – PCA 2 plane as shown in Fig.8. It is found that AE signals are well separated with clear boundaries and spatial distributions. This demonstrates the consistency of the clustering method employed in our analysis.

Using FFT method, the clusters spectrum information in the frequency-domain were obtained from the waveform information in the time-domain (Fig.9). It is found that the dominant frequency for CL-1, CL-2, and CL-3 clusters is about 100 kHz, 250 kHz, and 450 kHz, respectively. Previous studies investigated the relationship between AE frequencies and the damage mechanisms of composite materials [20,30,31,35,36]. It is found that the ranges of the dominant frequencies of matrix cracking, fiber-matrix debonding, and fiber breakage damages are about 100-200 kHz, 210-320 kHz and 390-460 kHz, respectively [20,30,31,35,36].

Thus, CL-1, CL-2, and CL-3 clusters with low, medium, and high frequencies mainly correspond to matrix cracking, fiber-matrix debonding, and fiber breakage, respectively. This indicates the strong correlation between AE clusters and the damage mechanisms. They also demonstrate the effectiveness of MPSA clustering approach in characterizing the damage mechanisms of hydrogen composite pressure vessels.

In addition, SEM microscopy was employed to observe the damage mechanisms on the burst pressure vessels. Macroscopic images of the vessels after burst and microscopic SEM images of the two vessels are presented in Fig.10a and Fig.10b. The figures clearly show the three damage mechanisms found in the current literature, which is consistent with the results of MPSA clustering analysis.

4.2 Damage evolution mechanisms

In Fig.11, the change in amplitude and pressure with time is studied for the hydraulic proof test (Fig.11a and Fig.11b) and burst test (Fig.11c and Fig.11d) for pressure ranges of 0-105 MPa and 0-158 MPa, respectively. The variation of AE signals with increasing pressure highlights the damage evolution mechanisms in the vessels.

According to Fig.11a and Fig.11b, only a few damage signals were initially obtained at 70 MPa. This can be explained by the elastic deformation of the vessel at this pressure. However, as the hydraulic proof test progresses, the signals increased slightly from 70 MPa to 105 MPa, which is mainly caused by matrix damage and fiber/matrix debonding. More significant damage is observed on the second vessel. This can be explained by its high fatigue cycles (7500 cycles) compared to the first vessel (5500 cycles). Similarly, Fig.11c and Fig.11d show that AE signals are initially insignificant at a pressure range of 70-105 MPa. This can be explained by the second loadings applied to the composite materials. These loadings were previously reached in the first loading 0-105 MPa of the hydraulic proof test. Thus, higher pressure is needed to create further damage. This also indicates that the damage is irreversible and that matrix damage, fiber-matrix debonding, and fiber breakage become significant at high pressures of 135 MPa, 150 MPa, and 158 MPa, consecutively.

In Fig.12, the variations of counts to peak and pressure with time are studied for the hydraulic proof test (Fig.12a and Fig.12b) and burst test (Fig.12c and Fig.12d). The pressure ranges are similar to those considered in Fig.11. With regards to the hydraulic proof test, Fig.12a

and Fig.12b show that signals associated with matrix damage correspond to a pressure range of 30-50 MPa and increase with increasing pressure. Similarly, Fig.12c and Fig.12d show that the pressure range for fiber-matrix debonding is mainly at a range of 100-130 MPa in the burst test, and the number of counts to peak signals for fiber-matrix debonding is smaller than that of matrix cracking. The fiber breakage damage has the least amount of signals located mainly near the highest pressure of 158 MPa. This indicates that the fiber breakage is mainly caused by high loading. These results are consistent with previous studies on the AE response of composite structures conducted by Pashmforoush et al. [30,31] and Mahdian et al. [35]. Thus, matrix cracking signals appear at low loading and their total amount during the loading process exceed other signals. The active loading distribution range for fiber-matrix debonding signals is generally greater than that for matrix cracking. Fiber breakage signals mainly appear at high applied loads and the amount of fiber breakage signals before ultimate failure is much less than that of the other damage modes. After conducting burst tests in a pressure range of 0-158 MPa, the vessels were re-pressurized to burst. The obtained burst pressure of vessels V1 and V2 are 168 MPa and 165 MPa, respectively. The damaged vessels due to burst-induced failure are shown in Fig.10, The vessels were shattered into several pieces. Around the cylinder part, matrix cracking, fiber-matrix debonding, and fiber breakage damage mechanisms can be clearly observed at the failure position.

5. Concluding remarks

The study presented in this paper consists in using an AE method to investigate the damage mechanisms of Type IV hydrogen pressure vessels with a service pressure of 70 MPa. AE signals were detected while conducting hydraulic proof test (pressure up to 105 MPa) and burst test (pressure up to 0-158 MPa) on two vessels using multi-step loading method. A multi-parameter statistical analysis (MPSA) based on empirical mode decomposition (EMD) and the *K*-means algorithm was employed to cluster the AE events. A relationship was found between AE features and the observed damage modes: the three MPSA clusters with separate amplitude, absolute energy, and energy were mainly correlated to three damage mechanisms namely, matrix cracking, fiber-matrix debonding, and fiber breakage. Also, the variation of AE feature

parameters with increasing pressure during the hydraulic proof and the burst tests was investigated and correlated to the damage evolution mechanisms observed on the vessels. Three main conclusions were obtained:

(a) The absolute energy, amplitude, energy, and counts to peak are applicable for the clustering of AE signals of composite hydrogen pressure vessels. The amplitude, absolute energy, and energy of the matrix cracking are generally the lowest, those associated with fiber breakage are the highest, and those corresponding to fiber-matrix debonding are in-between.

(b) AE signals at a pressure range of 70-105 MPa during the burst tests are insignificant. This can be explained by the second loadings applied to the composite materials, which were previously reached in the first hydraulic proof test loading (pressure up to 105 MPa). Higher pressure is needed to create further damage.

(c) The signals associated with matrix damage appear initially at low loading of 30-50 MPa, then increase with increasing pressure. More counts to peak were found for this damage is compared to fiber-/matrix debonding and fiber breakage damages. The active pressure range of fiber-matrix debonding signals is greater than that for matrix cracking. Also, signals associated with fiber breakage mainly appear near the highest pressure of 158 MPa and the amount of fiber breakage is much less than that of the two other damage modes before failure.

Acknowledgements

All authors sincerely appreciate the support of the National Key Research and Development Program of China (No. 2017YFC0805601) and National Natural Science Foundation of China (51675474).

References

[1] Zheng J, Zhao L, Ou K, Guo J, Xu P, Zhao Y, et al. Queuing-based approach for optimal dispenser allocation to hydrogen refueling stations. Inter J Hydrogen Energy 2014;39:8055-62.

[2] Son DS, Hong JH, Chang SH. Determination of the autofrettage pressure and estimation of material failures of a Type III hydrogen pressure vessel by using finite element analysis. Inter J Hydrogen Energy 2012;37:12771-81.

[3] Takeichi N, Senoh H, Yokota T, Tsuruta H, Hamada K, Takeshita HT, et al. “Hybrid hydrogen storage vessel”, a novel high-pressure hydrogen storage vessel combined with hydrogen storage material. Inter J Hydrogen Energy 2003;28:1121-9.

[4] Xu P, Zheng J, Chen H, Liu P. Optimal design of high pressure hydrogen storage vessel using

an adaptive genetic algorithm. Inter J Hydrogen Energy 2010;35:2840-6.
[5] Liu PF, Xing LJ, Zheng JY. Failure analysis of carbon fiber/epoxy composite cylindrical laminates using explicit finite element method. Compos Part B 2014;56:54-61.
[6] Bie H, Li X, Liu P, Liu Y, Xu P. Fatigue life evaluation of high pressure hydrogen storage vessel. Inter J Hydrogen Energy 2010;35:2633-26362008.
[7] Hong JH, Han MG, Chang SH. Safety evaluation of 70MPa-capacity type III hydrogen pressure vessel considering material degradation of composites due to temperature rise. Compos Struct 2014;113:127-33.
[8] Parnas L, Katırcı N. Design of fiber-reinforced composite pressure vessels under various loading conditions. Compos Struct 2002;58:83-95.
[9] Onder A, Sayman O, Dogan T, Tarakcioglu N. Burst failure load of composite pressure vessels. Compos Struct 2009;89:159-66.
[10] Gentilleau B, Villalonga S, Nony F, Galiano H. A probabilistic damage behavior law for composite material dedicated to composite pressure vessel. Inter J Hydrogen Energy 2015;40:13160-4.
[11] Son DS, Chang SH. Evaluation of modeling techniques for a type III hydrogen pressure vessel (70MPa) made of an aluminum liner and a thick carbon/epoxy composite for fuel cell vehicles. Inter J Hydrogen Energy 2012;37:2353-69.
[12] Dahmene F, Yaacoubi S, Mountassir ME, Langlois C, Bardoux O. Towards efficient acoustic emission testing of COPV, without Felicity ratio criterion, during hydrogen-filling. Inter J Hydrogen Energy 2016;41:1359-68.
[13] Poe C. Impact damage and residual tension strength of a thick graphite/epoxy rocket motor case. J Spacecraft Rockets 2015;29:394-404.
[14] ISO 11623: Transportable gas cylinders-Periodic inspection and testing of composite gas cylinders.
[15] Rosa IMD, Santulli C, Sarasini F. Acoustic emission for monitoring the mechanical behaviour of natural fibre composites: A literature review. Compos Part A 2009;40:1456-69.
[16] Chou HY, Mouritz AP, Bannister MK, Bunsell AR. Acoustic emission analysis of composite pressure vessels under constant and cyclic pressure. Compos Part A 2015; 70:111-20.
[17] Lin S, Jia X, Sun H, Sun H, Hui D, Yang X. Thermo-mechanical properties of filament wound CFRP vessel under hydraulic and atmospheric fatigue cycling. Compos Part B 2013;46:227-33.
[18] Oskouei AR, Zucchelli A, Ahmadi M, Minak G. An integrated approach based on acoustic emission and mechanical information to evaluate the delamination fracture toughness at mode I in composite laminate. Mater Des 2011;32:1444-55.
[19] Ni QQ, Iwamoto M. Wavelet transform of acoustic emission signals in failure of model composites. Eng Fract Mech 2002;69:717-28.
[20] Gutkin R, Green CJ, Vangrattanachai S, Pinho ST, Robinson P, Curtis PT. On acoustic emission for failure investigation in CFRP: Pattern recognition and peak frequency analyses. Mech Syst Signal Pr 2011;25:1393-407.
[21] Mccrory JP, Al-Jumaili SK, Crivelli D, Pearson MR, Eaton MJ, Featherston CA, et al. Damage classification in carbon fibre composites using acoustic emission: A comparison of three techniques. Compos Part B 2015;68:424-30.
[22] Han WQ, Ying L, Gu AJ, Yuan FG. Damage Modes Recognition and Hilbert-Huang Transform Analyses of CFRP Laminates Utilizing Acoustic Emission Technique. Appl Compos Mater

2016;23:155-78.
[23] Li L, Lomov SV, Yan X, Carvelli V. Cluster analysis of acoustic emission signals for 2D and 3D woven glass/epoxy composites. Compos Struct 2014;116:286-99.
[24] Marec A, Thomas JH, Guerjouma RE. Damage characterization of polymer-based composite materials: Multivariable analysis and wavelet transform for clustering acoustic emission data. Mech Syst Signal Pr 2008; 22:1441-64.
[25] GTR-13: United Nations Economic Commission for Europe Global Technical Regulation (GTR) Number 13: Proposal for a global technical regulation on hydrogen and fuel cell vehicles (ECE/TRANS/WP.29/AC.3/17).
[26] Huang NE, Shen Z, Long SR, Wu MC, Shih HH, Zheng Q, et al. The empirical mode decomposition and the Hilbert spectrum for nonlinear and non-stationary time series analysis. The Royal Society 1998; 454: 903-995.
[27] Hamdi SE, Duff AL, Simon L, Plantier G, Sourice A, Feuilloy M. Acoustic emission pattern recognition approach based on Hilbert–Huang transform for structural health monitoring in polymer-composite materials. Appl Acoust 2013;74:746-57.
[28] Huang T, Lou M, Chen H, Wang N. An orthogonal Hilbert-Huang transform and its application in the spectral representation of earthquake accelerograms. Soil Dyn Earthq Eng 2018;104:378-89.
[29] Das B, Pal S, Bag S. A combined wavelet packet and Hilbert-Huang transform for defect detection and modelling of weld strength in friction stir welding process. J Manuf Process 2016;22:260-8.
[30] Pashmforoush F, Fotouhi M, Ahmadi M. Damage characterization of glass/epoxy composite under three-point bending test using acoustic emission technique. J Mater Eng Perform 2012;21:1380-90.
[31] Pashmforoush F, Fotouhi M, Ahmadi M. Acoustic emission-based damage classification of glass/polyester composites using harmony search k-means algorithm. J Reinf Plast Compos 2012;31:671-80.
[32] Harčarik T, Bocko J, Masláková K. Frequency Analysis of Acoustic Signal using the Fast Fourier Transformation in MATLAB. Procedia Engineering 2012;48:199-204.
[33] Liu PF, Yang J, Wang B, Zhou ZF, Zheng JY. A study on the intralaminar damage and interlaminar delamination of carbon fiber composite laminates under three-point bending using acoustic emission. J Fail Anal Prev 2015;15:101-21.
[34] Li XK, Liu PF. Delamination analysis of carbon fiber composites under dynamic loads using acoustic emission. J Fail Anal Prev 2016;16:142-53.
[35] Mahdian A, Yousefi J, Nazmdar M, Zarif Karimi N, Ahmadi M, Minak G. Damage evaluation of laminated composites under low-velocity impact tests using acoustic emission method. J Compos Mater 2017;51:479-90.
[36] Nazmdar Shahri M, Yousefi J, Fotouhi M, Ahmadi Najfabadi M. Damage evaluation of composite materials using acoustic emission features and Hilbert transform. J Compos Mater 2016;50:1897-907.

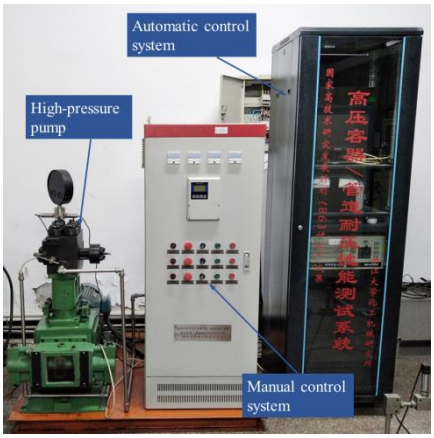

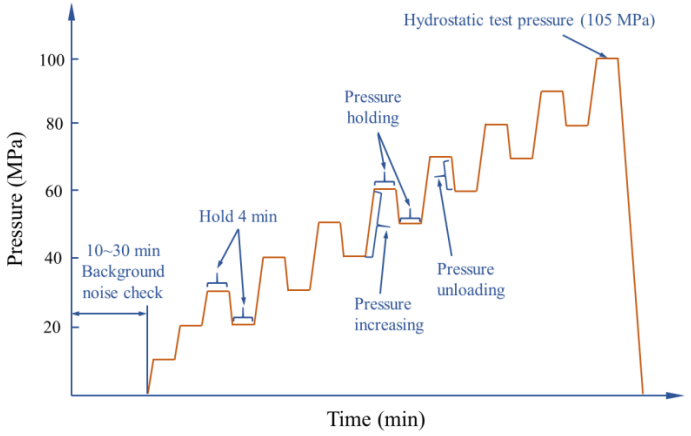

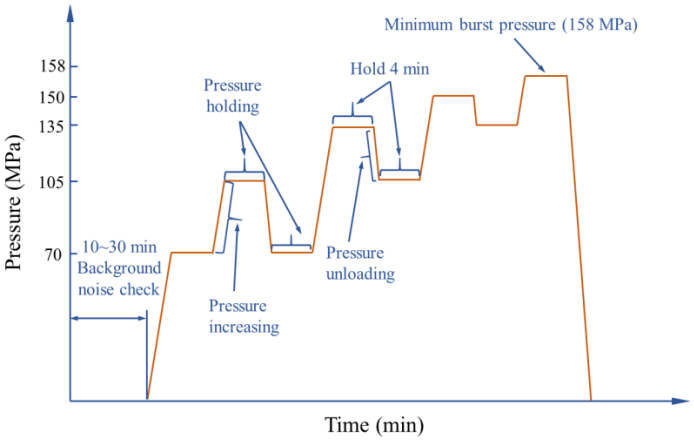

Fig.1 (a) Multifunctional pressure test system used for hydraulic proof test and burst test, (b) Multi-step loading method for hydraulic proof test and (c) Multi-step loading method for burst test.

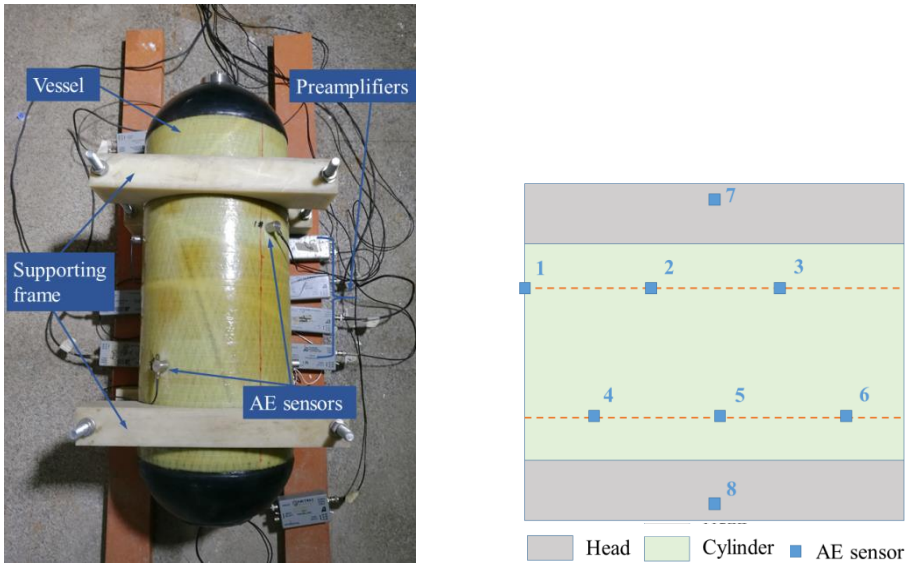

(a) (b)

Fig.2 (a) Vessels mounted with sensors and preamplifiers (b) Layout of the sensors on the vessels.

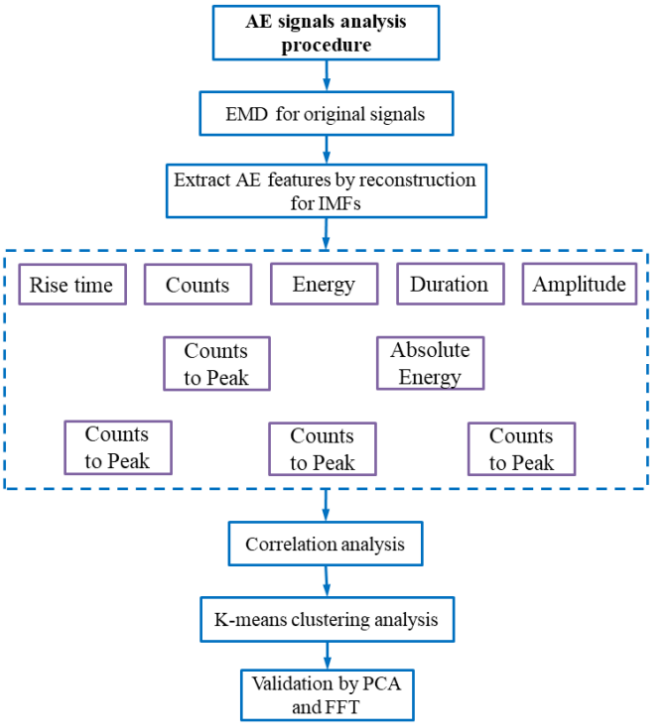

Fig.3 AE signals analysis procedure

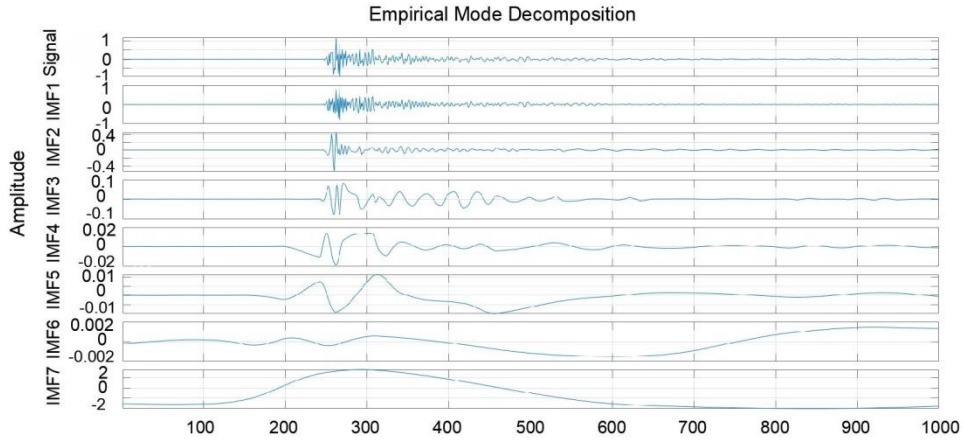

(a)

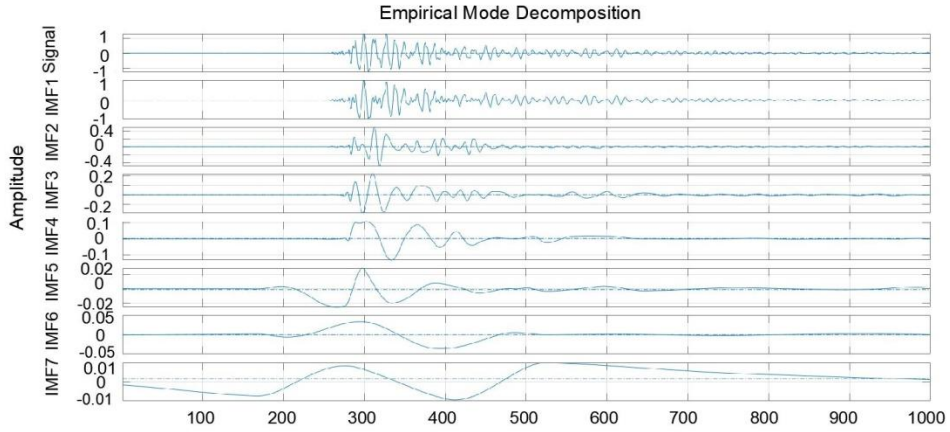

(b)

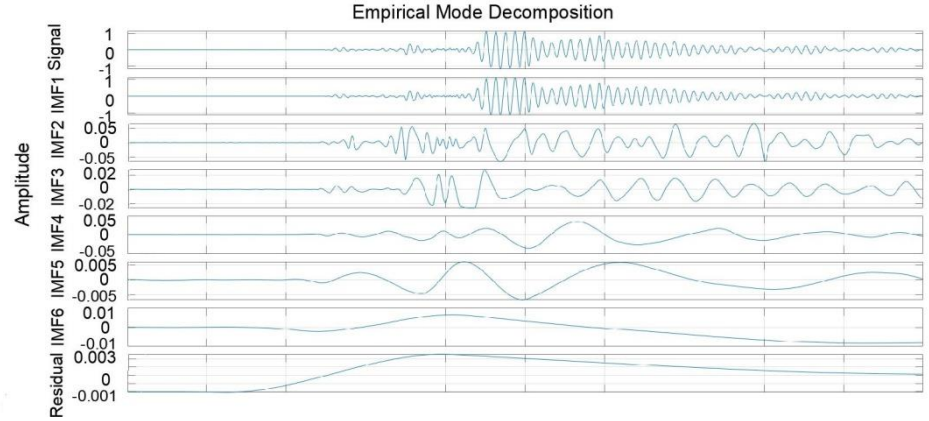

(c)

Fig.4 EMD-decomposed IMFs of AE signals with (a) low amplitude of 45 dB, (b) middle amplitude of 70 dB, and (c) high amplitude of 89 dB.

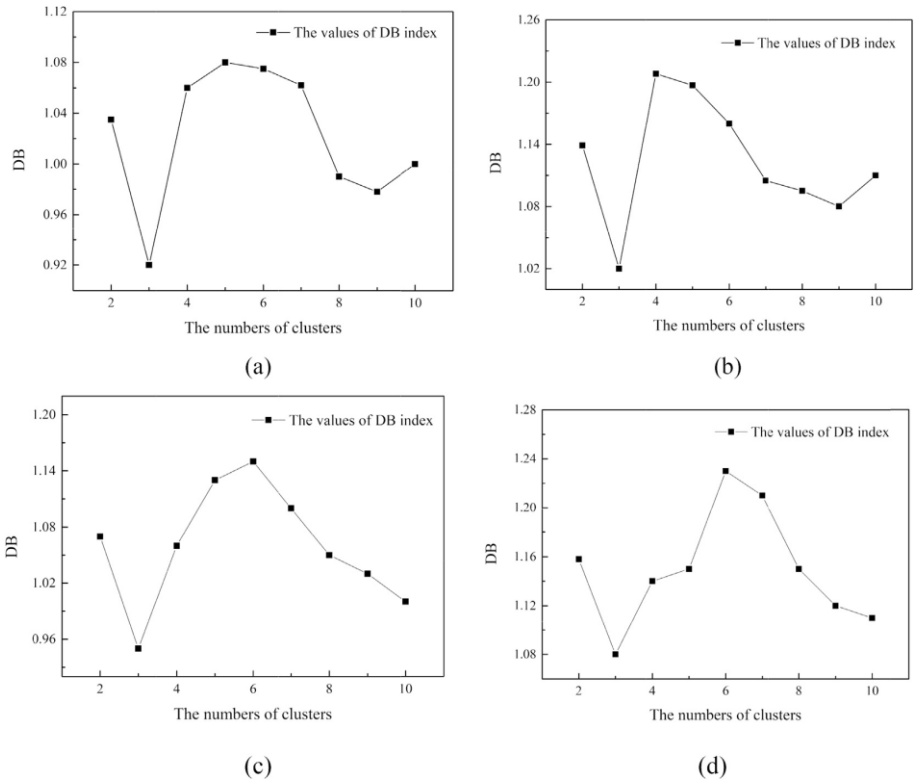

Fig.5 DB indexes of (a) V1-H, (b) V1-B, (c) V2-H and (d) V2-B tests

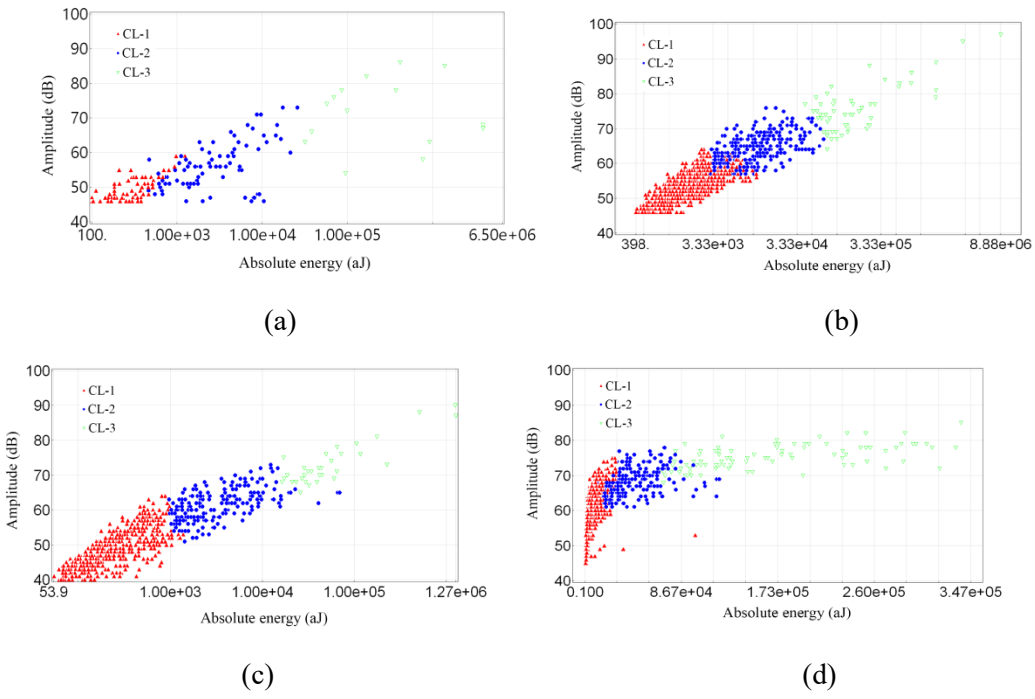

Fig.6 Correlated distribution between the amplitude and absolute energies for the AE signals of two vessels for (a) V1-H (b) V1-B (c) V2-H and (d) V2-B tests.

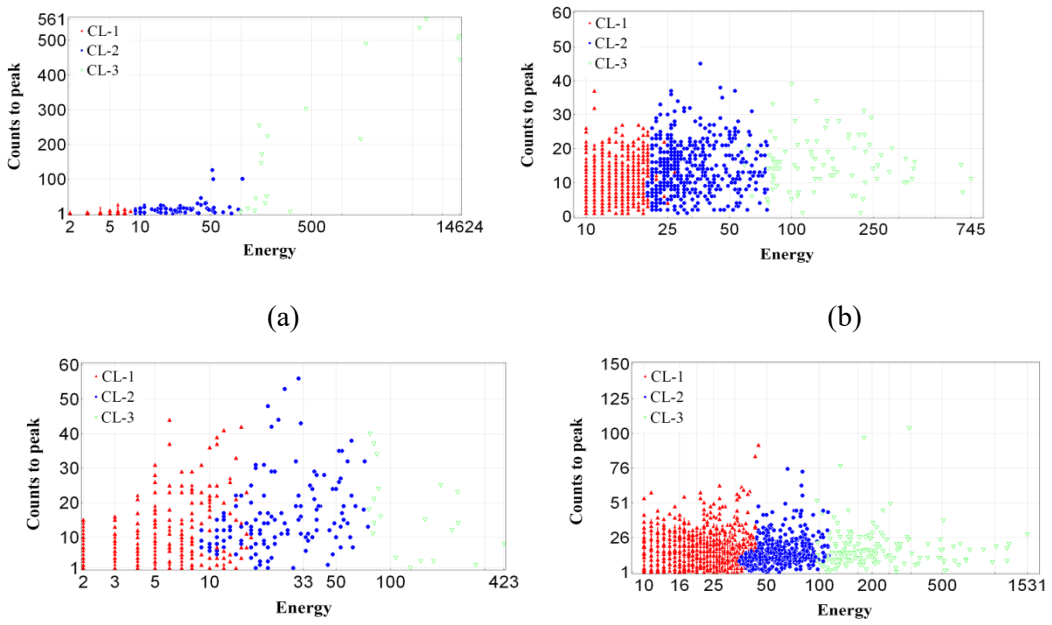

(a) (b)

(c) (d)

Fig.7 Correlated distribution between the counts to peak and energy parameters for AE signals of two vessels for (a) V1-H(b) V1-B (c) V2-H and (d) V2-B tests.

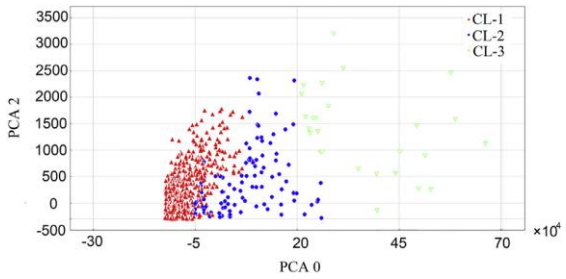

(a)

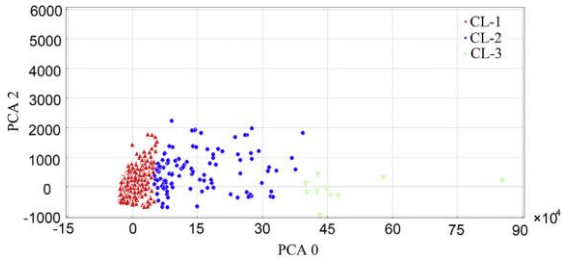

(b)

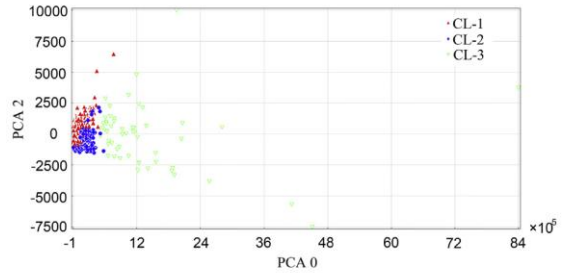

(c)

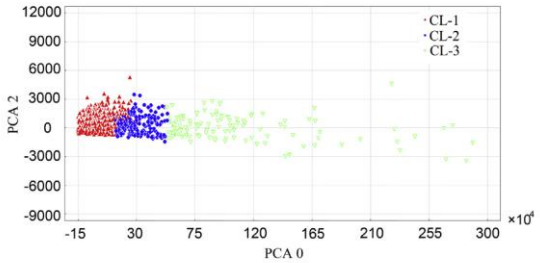

(d)

Fig.8 PCA visualization of *K*-means clustering results for (a) V1-H, (b) V1-B, (c) V2-H and (d) V2-B tests.

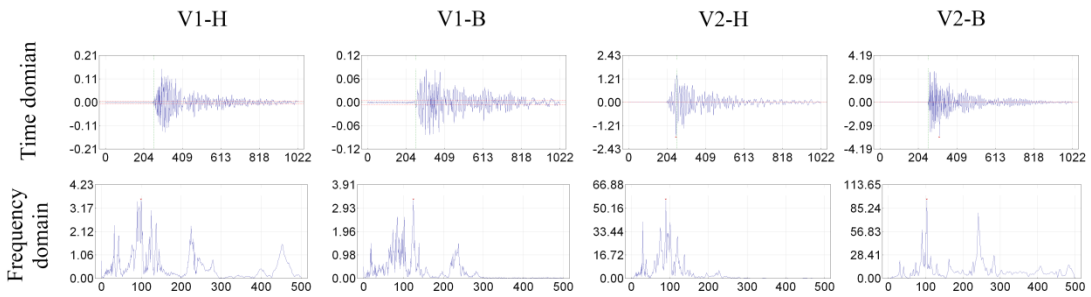

(a) CL-1 class

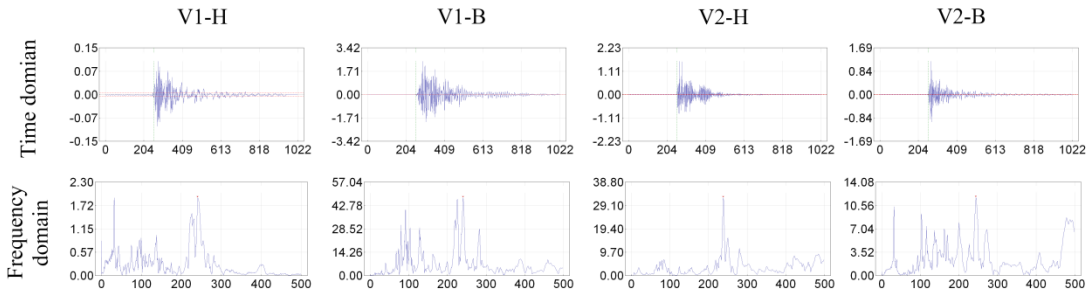

(b) CL-2 class

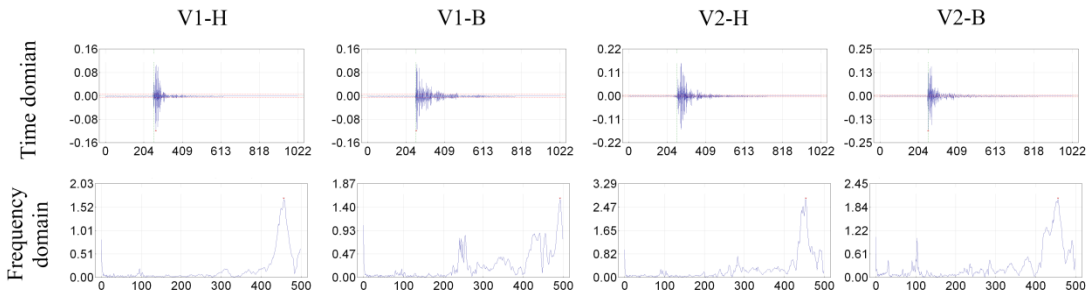

(c) CL-3 class

Fig.9 Time-domain (amplitude [mV] vs. time [s]) and frequency-domain (FFT amplitude [mV^2/Hz] vs. frequency [Hz]) results for clusters (a) CL-1, (b) CL-2, and (c) CL-3.

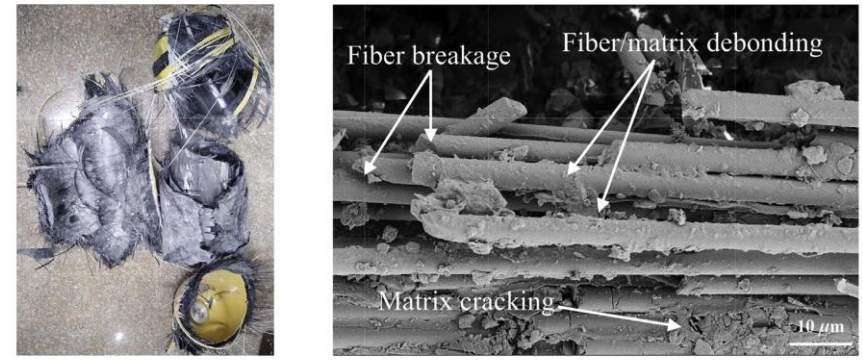

Fig.10 Burst status and SEM observation of damage mechanisms for (a) Vessel V1 and (b) Vessel V2.

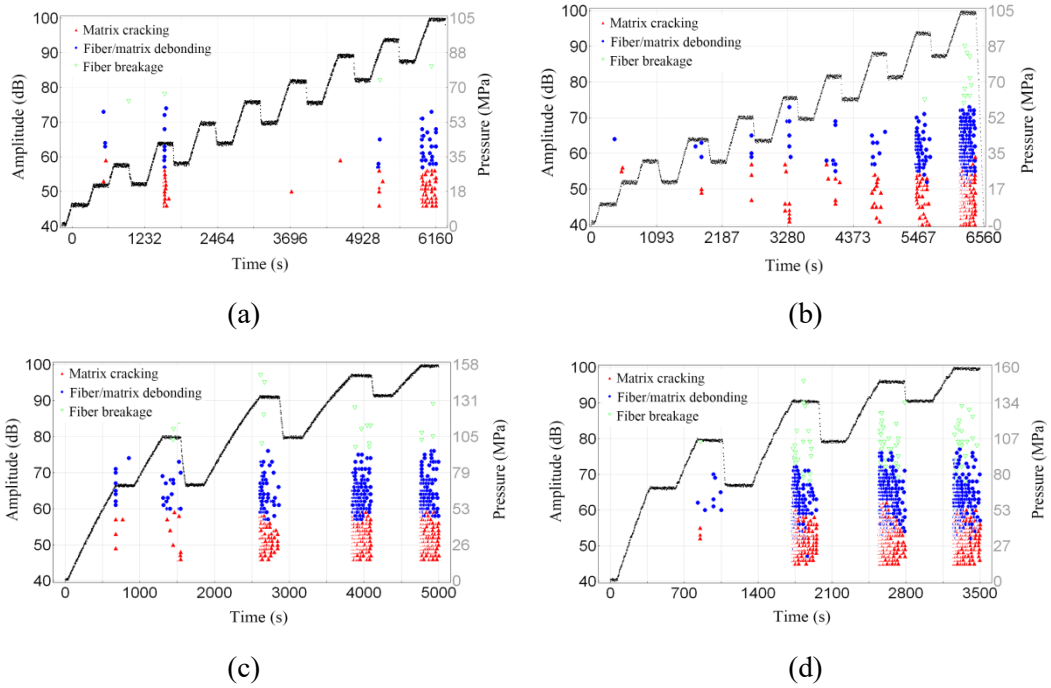

Fig.11 Variation of amplitude and pressure with testing time for (a) V1-H (b) V2-H (c) V1-B and (d) V2-B tests.

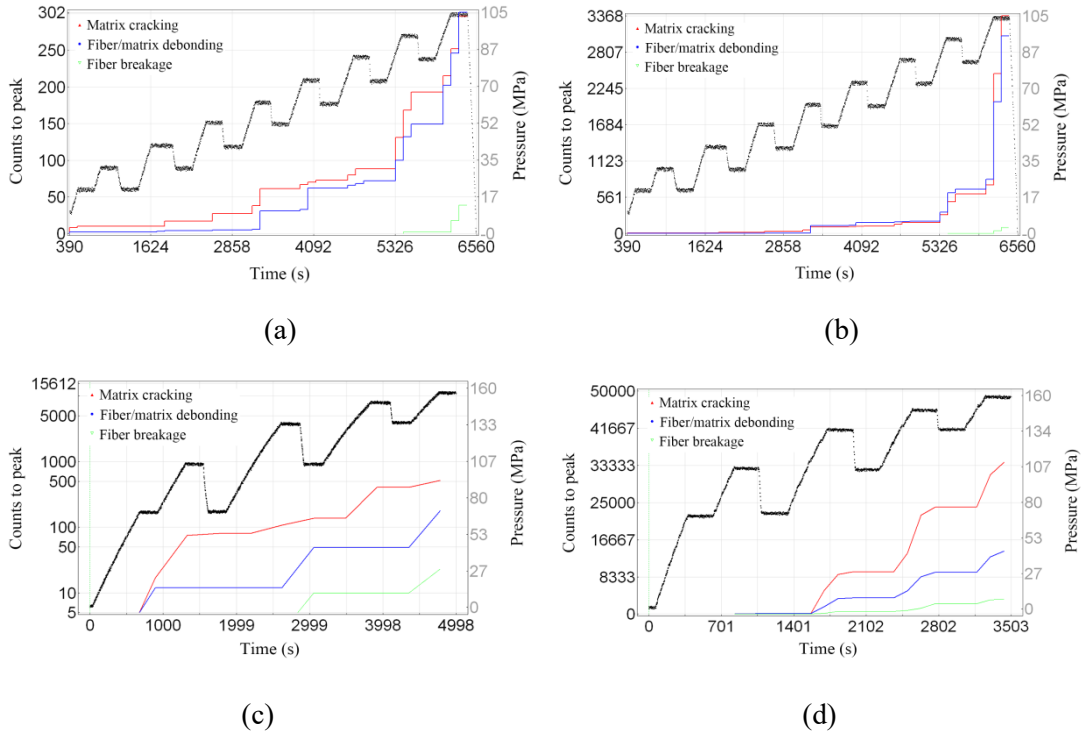

Fig.12 Variation of counts to peak and pressure with testing time for (a) V1-H (b) V2-H (c) V1-B and (d) V2-B tests.

Table 1 Pressure ranges of hydraulic proof and burst tests.

Vessel	Test	Pressure Range (MPa)	Initial Fatigue Cycles	Test Label
V1	Hydraulic Proof	0-105	5500	V1-H
V1	Burst	0-158	5500	V1-B
V2	Hydraulic Proof	0-105	7500	V2-H
V2	Burst	0-158	7500	V2-B

Table 2. Clustering results for hydraulic proof and burst tests for V1 vessel.

AE parameters	Hydraulic Proof Test			Burst Test		
	CL-1	CL-2	CL-3	CL-1	CL-2	CL-3
Amplitude (dB)	40-55	50-72	70-90	40-63	57-76	70-100
Absolute Energy (10^3 aJ)	0-2	2-40	＞40	0-3	3-60	＞60
Energy	0-10	10-100	＞100	0-20	20-90	＞90

Table 3. Clustering results for hydraulic proof and burst tests for V2 vessel.

AE parameters	Hydraulic Proof Test			Burst Test		
	CL-1	CL-2	CL-3	CL-1	CL-2	CL-3
Amplitude (dB)	40-65	55-72	65-90	40-70	62-80	75-90
Absolute Energy (10^3 aJ)	0-1	1-40	＞40	0-2	2-65	＞65
Energy	0-17	17-100	＞100	0-30	30-100	＞100